Structure
Article

Mechanistic Explanation of Different Unfolding Behaviors Observed for Transmembrane and Soluble β-Barrel Proteins

Ulf Hensen[1] and Daniel J. Müller[1,*]
[1]Department of Biosystems Science and Engineering, ETH Zurich, Mattenstrasse 26, Basel CH-4058, Switzerland
*Correspondence: daniel.mueller@bsse.ethz.ch
http://dx.doi.org/10.1016/j.str.2013.06.001

SUMMARY

In response to mechanical stress, membrane proteins progress through sequences of major unfolding barriers, whereas soluble proteins usually must overcome only one major unfolding barrier. To gain insight into these markedly different unfolding behaviors, we applied force-probe molecular dynamics simulations and unfolded two β-barrel proteins, the transmembrane outer membrane protein G (OmpG) and the water-soluble green fluorescent protein (GFP). The simulations mimic with high precision the unfolding experiments and show that OmpG in the absence of a membrane and GFP circumvent high unfolding barriers by rotations and explore alternative unfolding pathways. Embedding OmpG in the lipid membrane restricts this search for pathways and forces the protein to cross high unfolding barriers. Likewise, restricting the rotation forces GFP to traverse high unfolding barriers in a similar manner to membrane-embedded OmpG. These results indicate that mechanically stressed proteins search alternative unfolding pathways by rotations and explain why membrane proteins generally show higher mechanical stability compared to water-soluble proteins.

INTRODUCTION

Cellular membranes provide the compartmentalization required by living cells and embed specialized sets of membrane proteins that are uniquely adapted to cellular tasks such as solvent and ion exchange, molecular transport, energy conversion, sensing and signal transduction, cell adhesion, and response to mechanical stimuli. Transmembrane proteins are embedded in the cellular membrane where they form functional assemblies (Engelman, 2005; Lingwood and Simons, 2010; Coskun and Simons, 2011). Cellular membranes and assemblies of membrane proteins are continuously restructured depending on the functional state of the cell and are exposed to considerable mechanical stress caused by, for example, osmotic pressure, mechanical wear, or cell adhesion (Engelman, 2005; Haswell et al., 2011; Sheetz, 2001; Sukharev and Sachs, 2012). Membrane proteins can either adapt their functionality to this mechanical stress or must be able to withstand stress to maintain functionality. An interesting aspect of membrane proteins is that their mechanical properties are significantly different from those of water-soluble proteins, even if they have similar tertiary structures (Bosshart et al., 2012; Dietz and Rief, 2004; 2006; Sapra et al., 2009; Thoma et al., 2012). In the past, single-molecule force spectroscopy (SMFS) has been extensively applied to characterize the mechanical unfolding of various membrane and water-soluble proteins (Borgia et al., 2008; Engel and Gaub, 2008; Kedrov et al., 2007). The common observation is that membrane proteins are multistep (un)folders with each unfolding step formed by a major unfolding barrier. In contrast, water-soluble proteins (e.g., single protein domains) usually unfold in one major step, which suggests that only one major unfolding barrier separates the native from the random coiled state.

What is the reason for this difference? Among the more obvious explanations, exposure of the well-protected hydrophobic core of a water-soluble protein represents the all-dominant unfolding event (Onuchic and Wolynes, 2004). As soon as water enters the hydrophobic core, the unfolding protein destabilizes and the subsequent unfolding events are likely to require much less mechanical stress. This unfolding scenario contrasts with that experienced by proteins embedded in the cellular membrane. Upon exposure to a sufficiently high force, a membrane protein starts stepwise unfolding, with the unfolding intermediates remaining stabilized by the hydrophobic core and hydrophilic lipid headgroups of the membrane bilayer (Engel and Gaub, 2008; Kedrov et al., 2007). Furthermore, it is thought that an optimized hydrogen bond network significantly contributes to protein stability (Bowie, 2011). Compared to water-soluble proteins, the hydrogen bond network of a transmembrane protein is considerably strengthened by the hydrophobic core of a membrane bilayer that is characterized by a low dielectric constant and very little competitive hydrogen bonding (Bondar and White, 2012; Engelman et al., 2003; White and Wimley, 1999).

In this study, we applied atomistic force probe molecular dynamics (FPMD) simulations (Grubmüller et al., 1996; Isralewitz et al., 1997) to gain insight into the force-induced unfolding of two structurally similar water-soluble and membrane β-barrel proteins, the green fluorescent protein (GFP) from *Aequorea victoria* (Yang et al., 1996) and the outer (trans-)membrane protein G (OmpG) from *Escherichia coli* (Yildiz et al., 2006), respectively. Because both proteins have been extensively characterized by SMFS (Bertz et al., 2008; Damaghi et al., 2010b, 2011; Dietz and Rief, 2004, 2006; Mickler et al., 2007; Sapra

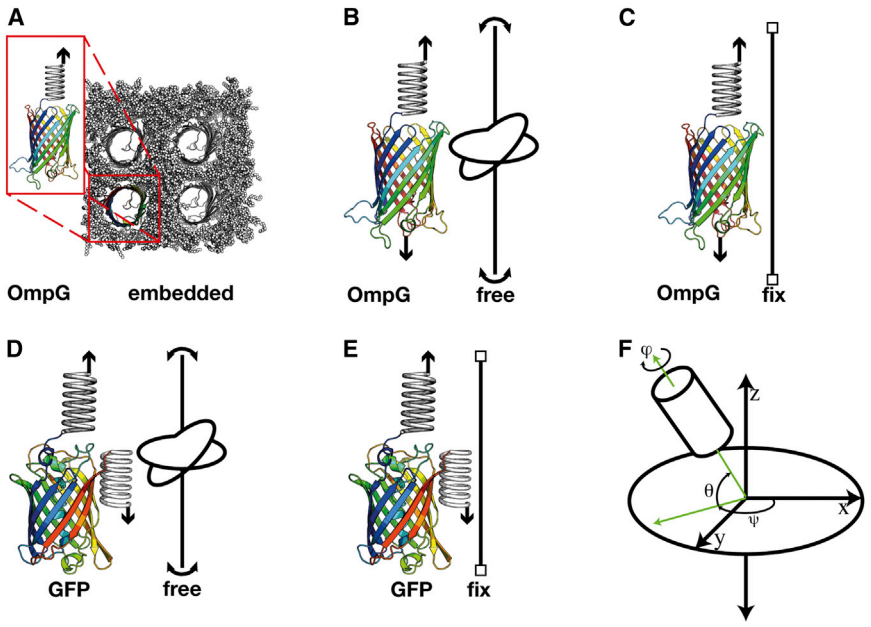

Figure 1. All-Atom FPMD Simulation Setups Used to Unfold the Transmembrane β-Barrel Protein OmpG and the Water-Soluble β-Barrel Protein GFP

(A) OmpG densely packed and embedded in a lipid (DMPC) membrane such as experimentally characterized by SMFS (Damaghi et al., 2010b, 2010a; Sapra et al., 2009). The red framed OmpG was mechanically pulled at the N-terminal end by the stylized spring.

(B) Solubilized OmpG that can rotate freely (curved arrows) in the absence of a membrane. In the absence of the anchoring lipid membrane, OmpG is pulled from N- and C-terminal ends.

(C) Solubilized OmpG mechanically pulled as in (B) but rotationally constrained to prevent molecular rotation.

(D) GFP mechanically pulled from N- and C-terminal ends such as experimentally characterized by SMFS (Dietz and Rief, 2004).

(E) GFP mechanically pulled as in (D) but rotationally constrained to prevent molecular rotation.

(F) Roll-pitch-yaw angle convention used to characterize rotation of the unfolding protein. All simulations were conducted in explicit water and ions (see Experimental Procedures) that are not shown for clarity. PDB entry files 2IWW (Yildiz et al., 2006) and 1GFL (Yang et al., 1996) were taken for OmpG and GFP, respectively.

et al., 2009), we are able to compare experiment and simulation in detail.

RESULTS AND DISCUSSION

FPMD Simulations Reveal Unfolding Pathways Similar to Experiment

First, we examined whether FPMD simulations reveal the same unfolding intermediates and pathways as previously inferred from SMFS experiments of OmpG and GFP (Bertz et al., 2008; Dietz and Rief 2004; Damaghi et al., 2011; Sapra et al., 2009). Therefore, as in the SMFS experiments, OmpG was embedded in a 1,2-dimyristoyl-sn-glycero-3-phosphocholine (DMPC) lipid bilayer, and we carried out six independent FPMD simulations (Figure 1; Figure S1 available online). In each FPMD simulation, we mechanically stressed the N-terminal end of a single OmpG and recorded the extension of the unfolding polypeptide in a so-called force-distance curve, as was the case in the SMFS experiments. These simulated force-distance curves could then be compared to force-distance curves recorded in SMFS experiments. The simulated force-distance curves revealed a number of pronounced force peaks, each describing an unfolding event of an individual OmpG (Figure S1). To analyze the general unfolding process of OmpG, we superimposed all simulated force-distance curves and calculated the average force-distance curve (Figure 2). This average force-distance curve shows the major unfolding force peaks common to most simulations (Figure S1). Due to the much stiffer cantilever used in the simulations, a number of minor force peaks, which were not detected in SMFS experiments (Figure S2), were observed between major force peaks (Figure S1). However, the structural unfolding intermediates of the average force-distance curve showed that each major force peak describes the unfolding of one β-hairpin formed by two β strands (Figure 2). Together, the seven major force peaks described the sequential unfolding of seven β-hairpins of the transmembrane β-barrel (Figure 2; Movie S1). As observed in the SMFS experiments (Figure S2), not all seven force peaks were detected in every simulated force-distance curve (Figure S1), which indicates that sometimes two β-hairpins unfolded in a single step (Sapra et al., 2009). The magnitude of the unfolding force peaks varied in the simulated force-distance curves such as experimentally recorded (Sapra et al., 2009). The ≈15 nm distances between the unfolding force peaks and the decreasing peak heights (Figure 2) agree quantitatively with the SMFS experiments (Figure S2X) (Sapra et al., 2009). Most important, the simulated unfolding pathway that describes the stepwise unfolding of the seven β-hairpins of the 14 β-stranded transmembrane β-barrel of OmpG closely resembles the pathway described from SMFS experiments (Sapra et al., 2009).

To investigate the unfolding pathway of a water-soluble β-barrel protein, we mechanically stressed both terminal ends of GFP (Figure 1D) in six independent FPMD simulations (Figure S3). The force-distance curves (Figure 2, blue) showed one early major force peak, after which no characteristic force peak was found. Structural unfolding intermediates showed that the major force peak corresponds to the opening of the hydrophobic β-barrel. After this unfolding event, the remaining structures of the β-barrel unfolded without crossing a significant unfolding barrier. This mechanical unfolding pathway is in agreement with SMFS experiments (Dietz and Rief, 2004) and in contrast to the unfolding pathway observed for OmpG (Sapra et al., 2009). Furthermore, the SMFS experiments quantified the unfolding forces of GFP to be 2-fold less than that of OmpG (110 versus 250 pN). This ratio was also found in our FPMD simulations, despite the unfolding forces of both β-barrel proteins being higher due to the application of higher pulling velocities.

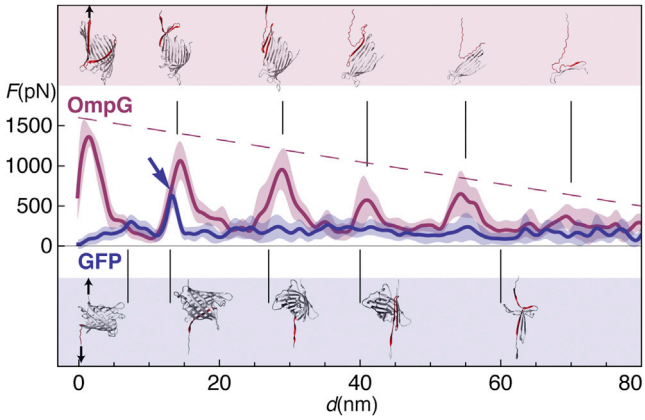

Figure 2. Average Force-Distance Curves and Unfolding Intermediates from All-Atom FPMD Simulations of OmpG Embedded in the Lipid Bilayer and of GFP

Each force-distance curve shows the average unfolding force (thick line) and SD (light area around average) from six independent simulations (Figures S1 and S3). Unfolding intermediates of OmpG (top, purple shaded background) and GFP (bottom, blue shaded background) show the unfolding segment, highlighted red. Vertical lines link the unfolding intermediates to the force-distance curve. Lipid bilayer, water and ions are not shown for clarity. Black arrows indicate the pulling direction of the mechanical force.

See also Figures S1–S3 and Movies S1 and S2.

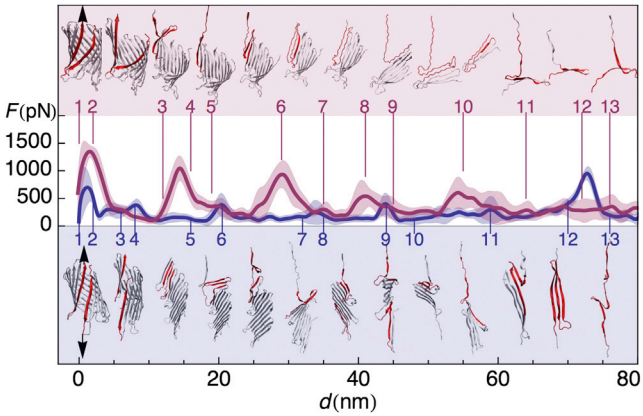

Figure 3. Average Force-Distance Curves and Unfolding Intermediates from All-Atom FPMD Simulations of OmpG in the Presence and in the Absence of a Lipid Bilayer

Each force-distance curve shows the average unfolding force (thick line) and SD (light area around mean) from six (Figure S1) or, respectively, three (Figure S4) independent simulations. Unfolding intermediates of OmpG in lipid bilayer (purple shaded background) and solubilized OmpG (blue shaded background) show the unfolding segments highlighted in red. Numbers located on force-distance curves correspond to the sequence of unfolding intermediates shown (from left to right). Lipid bilayer, water and ions are not shown for clarity. Black arrows indicate the pulling direction.

See also Figures S1, S4, and S8.

Unfolding Force Depends on the Orientation of the β-Barrel

While the FPMD simulations confirmed the experimentally observed unfolding pathways, they did not explain why the two β-barrel proteins unfold so differently. Close structural inspection of the FPMD trajectories suggests that the force required to extract β-hairpins of OmpG lessens as the transmembrane β-barrel starts tilting away from its initially upright position (Figure 2). The final unfolding force peak at a distance ≈70 nm, which is barely present in the mean OmpG spectrum, occurs when the remaining β-hairpin has completed a 90° rotation and lies on the membrane surface (Figure 2, rightmost snapshot). These rotations suggest that the unfolding forces correlate with the orientation of the unfolding intermediate. It has been shown that β strands oriented perpendicular to the pulling direction rupture at relatively low force, whereas β strands oriented parallel to the pulling direction rupture at higher forces (Gräter et al., 2005). Indeed, the simulated unfolding trajectories of GFP show that the water-soluble β-barrel reorients when exposed to an external pulling force. In most cases, the unfolding β-barrel orients perpendicular to the applied mechanical stress so that β sheets unfold in a zipper-like fashion, which requires much less force (Figure 2; Movie S2).

In Absence of the Lipid Bilayer OmpG Unfolds Similar to GFP

Next, we asked to what extent the higher mechanical stability of OmpG unfolding intermediates is due to the protein being embedded in the lipid membrane. To answer this question, we simulated the mechanical unfolding trajectories of OmpG in the absence of the lipid membrane (Figure 1B). Most outer membrane proteins (Omps) from *E. coli* show considerable kinetic and thermal stability, which enables their investigation in the solubilized state by conventional biochemical experiments (Bonhivers et al., 2001). Accordingly, within the timeframe of FPMD simulations (≈200 ns), OmpG did not unfold spontaneously in the absence of a lipid bilayer. The simulated unfolding force-distance curve of solubilized OmpG (Figure 3) shows a prominent force peak that correlates to the opening of the β-barrel. Thereafter, with a single exception, all unfolding force peaks are significantly weaker than the unfolding force peaks simulated for membrane-embedded OmpG (cf. Figure 2). The notable exception is the last unfolding force peak at a pulling distance of ≈72 nm, which is higher for solubilized OmpG than for OmpG in the lipid membrane (Figure 3). In unfolding events subsequent to the first, which opens the β-barrel, the individual β strands rotated 45° relative to the pulling direction. This rotation enables the zipper-like unfolding of β strands at lower forces. At a pulling distance of ≈70 nm, at which point most of the β-barrel has been unfolded, this rotation changes and the remaining three β strands aligned parallel to the pulling direction. As a result, the last unfolding force peak is significantly higher than the preceding ones. Apart from the last unfolding force peak, the unfolding force-distance spectra of solubilized OmpG is similar to the GFP spectra: Upon exposure to mechanical stress, the unfolding β-barrel freely rotates so that β strands unfold in a zipper-like manner and, thus, at low applied force. Such free rotation is restricted for proteins embedded in lipid membranes.

Rotationally Confined GFP Unfolds Similarly to Membrane-Embedded OmpG

In the previous section, we described that, in absence of a lipid bilayer, OmpG unfolds similarly to GFP. Next, we investigated whether rotationally confined GFP unfolds similarly to OmpG

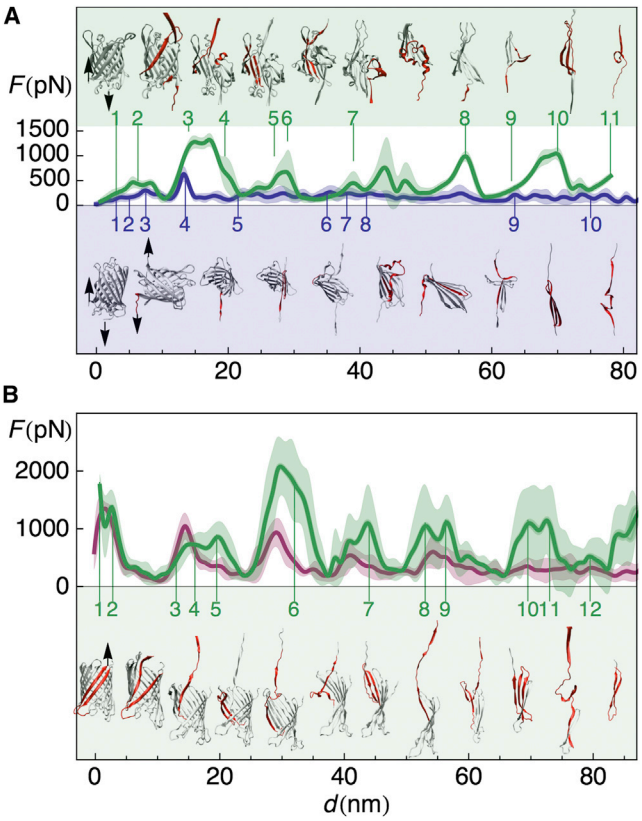

Figure 4. Average Force-Distance Curves and Unfolding Intermediates of Rotationally Free and of Rotationally Constrained GFP and OmpG

(A) Average unfolding force-distance curves of rotationally free GFP (blue) and of rotationally constrained GFP with fixed pitch angle θ (green).

(B) Average unfolding force-distance curves of OmpG embedded in membrane (purple) and of rotationally constrained solubilized OmpG with fixed pitch angle θ (green). Numbers located to force-distance curves correspond to the sequence of unfolding intermediates shown (from left to right). Unfolding segments of unfolding intermediates are highlighted in red. Each force-distance curve has been averaged from at least three individually simulated single force-distance curves of free OmpG (Figure S4), of rotationally constrained GFP (Figure S6), of OmpG embedded in the lipid bilayer (Figure S1), or of rotationally constrained solubilized OmpG (Figure S5). Averaged force-distance curves (thick line) and SDs are shown (light area around average force). Black arrows indicate the pulling direction.

See also Figures S1 and S4–S6 and Movies S3 and S4.

confined and embedded by the lipid membrane. To this end, we simulated the mechanical unfolding of GFP in solution but confined the rotation of the β-barrel (Figure 1E) by applying a time-invariant rotational potential throughout the FPMD simulation (Experimental Procedures) (Kutzner et al., 2011). This potential confined the rotation of GFP during the FPMD simulation just as a lipid membrane confines the rotation of OmpG. The simulated force-distance curves of confined GFP showed series of pronounced unfolding force peaks (Figure 4A; Movie S3) that were not present in unfolding curves of rotationally free GFP (Figure 4A). Notably, the unfolding force peaks of rotationally confined GFP occurred at distances similar to the unfolding force peaks measured from membrane-embedded OmpG (Figure 3), a consequence of the β strands in GFP and OmpG being of similar lengths. Some force peaks measured from confined GFP were even higher than unfolding force peaks from membrane-embedded OmpG. The height of the unfolding force peaks of rotationally confined GFP increased by an average of ≈850 pN (≈2-fold). This is surprising because our FPMD simulations artificially confined the rotation of GFP in the absence of a lipid bilayer and thus omitted any stabilizing effects that may strengthen hydrogen bonds in membrane proteins such as OmpG. Furthermore, the unfolding spectra of rotationally confined GFP revealed significantly more structural details than the unfolding spectra recorded from free GFP (Figure 4A).

Next, we simulated the unfolding of solubilized OmpG by applying the same rotational confinement as above for GFP (Figure 4B; Movie S4). The resulting force-distance curves of solubilized and confined OmpG show pronounced unfolding force peaks at similar positions as in membrane-embedded simulations. It is interesting that, whereas the first unfolding force peaks of rotationally confined OmpG are of similar height as those observed for membrane-embedded OmpG, the later force peaks are markedly higher. These simulations show that rotational freedom is important in shaping the unfolding pathways of water-soluble and of membrane proteins.

Reconstructing the Unfolding Energy Landscape of Rotationally Free and Confined β-Barrel Proteins

Our simulations indicate that the magnitude of unfolding force peaks of membrane-embedded OmpG decreases sequentially because the membrane loses its grip on the unfolding β-barrel. In contrast, an external rotational potential mimicking the perfect grip of a "virtual membrane" never allows tilting of the unfolding β-barrel. Consequently, β-hairpins of a rotationally confined β-barrel remain parallel to the pulling direction, and their unfolding requires more force. These observations support the hypothesis that, in the case of a freely rotating protein, most of the high unfolding energy barriers were not probed under load, because the unfolding β-barrel was able to circumvent them by rotations. Figure 5A illustrates the mechanical unfolding energy landscape of membrane-embedded and solubilized OmpG. To quantify the rotation of OmpG during the unfolding process, we monitored the Euler angles as a function of end-to-end distance (Experimental Procedures). As the pitch angle θ is the only angle restrained in the rotationally confined FPMD simulations, we take this angle as the angular coordinate. Consequently, the unfolding pathways along the unfolding energy landscape are governed by a distance- and rotation angle-dependent unfolding energy potential V, which we approximated based on the simulation data (Experimental Procedures). The unfolding pathways from native state (minimum state at bottom of landscape) to unfolded state (outer rim of landscape) are displayed on the surface of the unfolding energy landscape and, for unobstructed view, as projection on the bottom of Figure 5 (dashed lines). The unfolding energy landscape shows that OmpG embedded into a lipid membrane has no choice other than to probe all energy barriers between the native state and the unfolded state (Figure 5A, purple unfolding pathway). In contrast, solubilized OmpG circumvents most of the high energy barriers by deviating from the unfolding pathway of membrane-embedded OmpG and reorients by as much as 90° (from −45° to +45°) thereby reducing

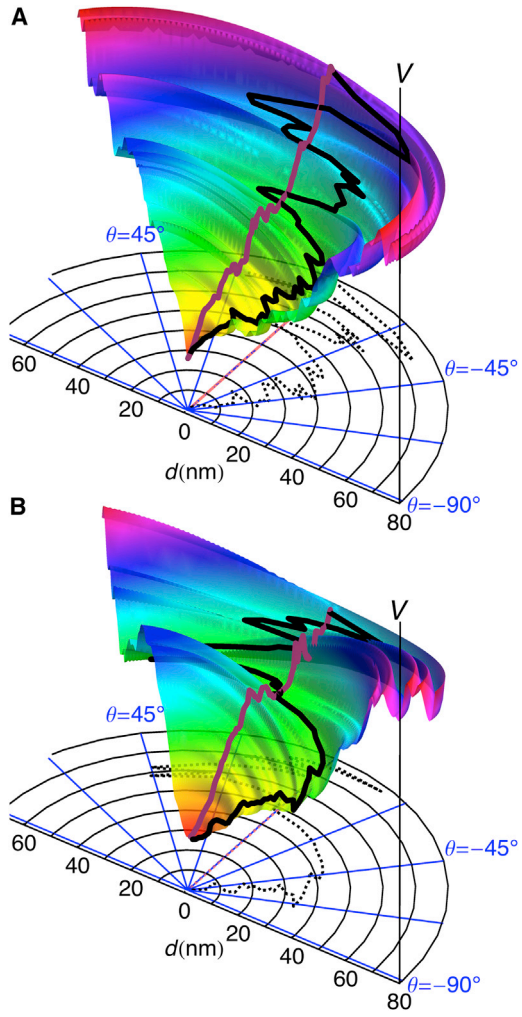

Figure 5. Unfolding Energy Landscape of OmpG and GFP

(A) Unfolding energy landscape of OmpG as a function of pulling distance d and pitch angle θ (see Experimental Procedures). The energy $V(d, \theta)$ was approximated by the θ-weighted average of the integrals of force-distance curves simulated for OmpG embedded in the lipid membrane (purple) and for solubilized rotationally free OmpG (black) (Figure 3). The unfolding pathways correlate to the ones shown in Figure 3. At fixed pitch angle θ, OmpG embedded in the lipid membrane is forced to probe all unfolding energy barriers on its way out of the (un-)folding energy landscape. In contrast, solubilized OmpG angularly reorients to circumvent most unfolding energy barriers.

(B) Unfolding energy landscape of rotationally constrained (purple) and free (black) GFP. GFP with the pitch angle θ rotationally constrained at zero (cf. Figure 4A) probes all unfolding energy barriers from the folded state (d = 0 nm) to the fully extended unfolded state. Rotationally free (variable θ) GFP subjected to mechanical load rotates around most unfolding energy barriers. The unfolding pathways correlate to the ones shown in Figure 4A. Positions indicating unfolding intermediates along the unfolding pathways are shown in Figure S8.

See also Figures S7 and S8.

the mechanical load required to unfold the β-barrel (Figure 5A, black unfolding pathway).

Similar pathways along the unfolding energy landscape are obtained by following the aforementioned protocol for rotationally free and rotationally restrained GFP (Figure 5B). Whereas GFP fixed in an upright orientation probes all high energy barriers between native and unfolded state (Figure 5B, purple unfolding pathway), the free GFP escapes mechanical load by rotating around these barriers (Figure 5B, black unfolding pathway). It is interesting that GFP performs much more pronounced rotations than solubilized OmpG, zigzagging back and forth between $\theta = -67.5°$ and $\theta = 45°$ (Figure 5B, dashed projection of unfolding pathway). This difference is due to topological differences between OmpG and GFP. Whereas the OmpG β-barrel is formed only by β-hairpins (Yildiz et al., 2006), the GFP β-barrel encloses an α-helix that interrupts the sequential order of the β-hairpins (Yang et al., 1996). Therefore, whereas, for OmpG, rotations of less than 45° in either directions proved sufficient to allow zipper-like unfolding of the individual β-hairpins, for GFP, much larger rotations were required. In terms of the energy landscape, the energy wells of GFP are significantly broader than those of OmpG, and to traverse these energy wells during unfolding requires GFP to move further along the angular coordinate.

Conclusions

We addressed the question of why membrane proteins subjected to mechanical load behave so differently from soluble proteins. To this end, we carried out FPMD simulations to investigate the unfolding behavior of two β-barrel proteins, GFP and OmpG, that have both been extensively studied by SMFS. These SMFS experiments revealed that the β-barrel of OmpG sequentially unfolds one β-hairpin after the other with each unfolding step being clearly detected by a single unfolding force peak. In contrast, GFP unfolds via one major unfolding step (force peak) corresponding to the opening of the β-barrel. The common explanation for this difference was that the hydrophobic core of OmpG and embedding lipid bilayer strengthens the hydrogen bonding of secondary structure elements in a way that the protein becomes more resistant to mechanical load. Our FPMD simulations reproduced the unfolding pathways of OmpG and GFP observed experimentally by SMFS. However, contrary to our initial expectations, the simulations showed that OmpG and GFP unfolded differently because the lipid bilayer held OmpG in an upright position and restricted its reorientation under mechanical load. In contrast, upon exposure to mechanical load, the unfolding GFP continuously reoriented so that each secondary structure element experienced least load as it unfolded. This rotational search for the lowest unfolding energy barrier was efficient so that unfolding of the unfolding intermediates of GFP could no longer be detected by force spectroscopy.

Our results further demonstrate that the apparent single-step unfolding process observed for water-soluble proteins by SMFS can be misleading. In truth, these proteins unfold sequentially in the same way that membrane proteins do. The reason that only one or two unfolding events can be observed by SMFS is that water-soluble proteins, when put under mechanical load, circumvent unfolding free energy barriers by continually rotating into energetically favorable orientations. This rotation under mechanical load is determined by the structure of the unfolding intermediate and allows the unfolding intermediates to curve around major unfolding energy barriers in the search for lower ones. Conversely, and in contrast to previous speculations about possible stabilizing roles of the lipid bilayer, the reason why SMFS measures many more unfolding intermediates in

membrane proteins than in water-soluble proteins (Bippes and Muller, 2011; Engel and Gaub, 2008; Kedrov et al., 2007) is that the membrane restrains the rotation of the embedded proteins. Accordingly, when rotationally restrained, the stepwise unfolding of water-soluble GFP could be clearly detected in force-distance curves and the characteristic unfolding intermediates of OmpG were not captured by SMFS when the protein was allowed to rotate freely.

An interesting structural feature of many proteins that have to resist mechanical forces in nature is that their structure prevents rotation under mechanical stress, such as is the case for titin kinase (Gräter et al., 2005; Puchner et al., 2008) or ankyrin (Lee et al., 2006, 2012). When exposed to biologically relevant forces, such proteins can resist high mechanical load because their tertiary or quaternary structure prevents rigid body rotation (Nunes et al., 2010), thereby preventing consecutive hydrogen bond breakage. We propose that SMFS assays, which aim to characterize the unfolding intermediates of proteins, should be set up so that rigid-body rotations are prevented, i.e., by framing with nanobodies or membranes, or by scaffolding proteins. Alternatively, proteins may be engineered to become mechanically more stable by restraining their rigid-body rotations. As the mechanical stability of proteins is of importance for many biotechnological applications, such "molecular framing and stabilization" of proteins may soon be realized.

Another conclusion derived from our results concerns the common way of interpreting dynamic single-molecule force spectroscopy data to derive positions and heights of energy barriers of the unfolding free energy landscape (Dudko et al., 2003, 2006; Evans, 1998, 2001; Evans and Ritchie, 1997). Here, the underlying assumption is that the distance of the folded to the unfolding energy barrier corresponds to a linear pathway on the unfolding free energy landscape. For most soluble proteins, this assumption must be reconsidered because their rotation changes the unfolding pathway, i.e., the unfolding energy barrier crossed.

EXPERIMENTAL PROCEDURES

Generation of Structures for Simulations

X-ray crystal structures for GFP (Protein Data Bank [PDB] ID 1GFL) (Yang et al., 1996) and OmpG (PDB ID 2IWW) (Yildiz et al., 2006) were obtained from the PDB (Berman et al., 2000; Bernstein et al., 1977). In both cases, the first of two chains present in the crystal structures was used. Gaps and missing side chain atoms were refilled using the molecular modeling program WHAT IF (Vriend, 1990). The hydrogen bond network was optimized as described in Hooft et al. (1996) and used to determine optimal rotamer angles and protonation states for Asn, His, and Gln residues. Aromatic groups with unphysical deviation from planarity were changed into planar conformation. All simulations were carried out using the molecular dynamics suite GROMACS (Berendsen et al., 1995; Hess et al., 2008) using the Optimized Potentials for Liquid Simulations (OPLS) force field (Jorgensen and Tiradorives, 1988). To rule out incorrect conclusions due to force field issues, we used the AMBER ff99sb*-ildn (Lindorff-Larsen et al., 2010) force field for comparison.

To set up FPMD simulations (Figure 1A), OmpG was embedded in a recently published DMPC Berger lipid (Berger et al., 1997) bilayer (Tieleman, 2011). The membrane patch was duplicated in the x and y directions using the GROMACS tool genconf (Hess et al., 2008), yielding a 11 nm × 11 nm large membrane. Four OmpG molecules were embedded piecewise into the membrane patch using g_membed (Wolf et al., 2010) at mutual distances to mimic densely packed OmpG membranes experimentally described by high-resolution atomic force microscopy (Mari et al., 2010). Then, the simulation box was extended in the z direction to 27 nm and filled with SPC/E—extended simple point charge—water molecules and sodium and chloride ions (c = 0.15 mol/l). The system was energy minimized in 1,400 steps by steepest descent, followed by an isothermic-isochoric equilibration of water and protein side chains for 2 ns with protein heavy atoms and lipids subjected to positional restraints (force constant, 1,000 kJ mol^{-1} nm^{-2}). Protein, lipid, and water were coupled separately to a V-rescale external heat bath (Bussi et al., 2007) with $\tau_T = 0.1$ ps. Subsequently, an isothermic-isobaric (NPT) equilibration of 2 ns length without any positional restraints was carried out with protein, lipid and water coupled separately to a Nosé-Hoover thermostat (Hoover, 1985; Nosé, 1984) with $\tau_T = 0.5$ ps and semi-isotropically to a Parrinello-Rahman barostat (Parrinello, 1981) at 1 bar with $\tau_p = 5$ ps. Application of LINCS (Hess et al., 1997) and SETTLE (Miyamoto and Kollman, 1992), combined with virtual interaction sites for hydrogens (Hess et al., 2008) allowed simulation time steps up to 4 fs. Short-range electrostatic and Lennard-Jones interactions were computed within a cutoff of 0.9 nm, and the neighbor list was updated every five steps. The particle mesh Ewald method (Darden et al., 1993) was used for long-range electrostatic interactions with a grid spacing of 0.16 nm and cubic interpolation.

FPMD simulations were carried out, with the C-terminal C-α atom as pull group and the lipid bilayer as reference group. For this setup, the large membrane patch and the neighboring OmpG monomers provided a sufficient stable scaffold to prevent the extraction of the membrane protein. Additional statistics at lower computational cost were obtained by proceeding analogously to the procedures described in the previous paragraph but embedding only one OmpG monomer into the membrane patch (Figure 1A, inset). Because of the small size of the membrane patch, OmpG happened to be pulled out from the lipid bilayer at early stages. To exert slightly more mechanical load on the protein instead of the membrane, the lipid bilayer together with residue GLY 13 in the first N-terminal loop were used as FPMD reference group.

For FPMD simulations, GFP was embedded in a triclinic box of dimensions 7 nm × 7 nm × 23 nm (Figures 1B and 1D). The equilibration process was identical to that described for OmpG, except for the NPT equilibration, where a isotropic Berendsen barostat (Berendsen et al., 1984) was used instead of a semi-isotropic Nosé-Hoover barostat. Subsequent FPMD simulations proceeded as described later. FPMD setups in Figures 1C and 1E were identical to those in Figures 1B and 1D, but during simulations, the protein orientation was kept upright by application of an additional rotational potential (see FPMD Simulations with Rotational Restraints).

FPMD Simulations

To mimic SMFS experiments, FPMD simulations were carried out (Grubmüller et al., 1996; Isralewitz et al., 1997). In these simulations, a harmonic spring potential was attached to a selected subset of atoms (referred to as the "pull group"), described by

$$V_{\mathrm{spring},i}(t) = \frac{k_0}{2}\left(z_i - z_{\mathrm{spring},i}(t)\right)^2,$$

where $k_0 = 500$ kj mol^{-1}nm^{-2} (0.83 N/m) is the force constant of the spring, z_i is the position of atom i relative to some reference subset of atoms (referred to as the "reference group"), and $z_{\mathrm{spring},i}$ is the position of the harmonic spring attached to atom i. The spring was then moved with constant velocity, $v = 0.4$ m/s, so that $z_{\mathrm{spring},i}(t) = z_i(0) + vt$. Because of the moving spring, the pulled atoms experienced a mechanical force, $F_i(t) = k_0(z_i - z_{\mathrm{spring},i}(t))$, which was monitored during the simulations and plotted in Figures 2, 3, and 4. The GROMACS direction_periodic FPMD algorithm was used with zero box compressibility in the pulling direction. To avoid possible artifacts due to the periodic boundary conditions, simulations were interrupted before the molecular extension exceeded the box length, unfolded residues removed, and the simulation continued with a new reference atom i closer to the still folded protein body, after an equilibration procedure as described earlier. To ensure that this procedure did not produce any artifacts, for each setup listed in Figure 1, at least one simulation was carried out with a box long enough to accommodate the fully unfolded proteins. For OmpG in solution (Figure 1B), the cutting approach was not feasible without cutting off still folded secondary structure elements. Here, only two simulations (with Amber and OPLS) in a box long enough to accommodate the unfolded proteins (105 nm) were carried out.

To generate statistically independent unfolding trajectories, for each setup five equidistant ($\Delta t = 400$ ps) snapshots were taken from NPT equilibration simulations described earlier. Each of these equidistant snapshots was used as starting structures for FPMD simulations.

Averaging of Force-Distance Curves

To calculate their average, we merged single force-distance curves and binned them into 1 nm wide bins. For each bin, the average force and the SD were computed and plotted after smoothing with an interpolation polynomial of degree 3. Accordingly, the force-distance curves presented in Figures 2–4 show the mean of several (number given for each case) independent unfolding force-distance curves (solid line) as well as the SD (shaded area). Force-distance curves in Figures 2–4 were prepared using mathematica 8.0 (Wolfram Research, Inc., 2010).

FPMD Simulations with Rotational Restraints

To keep the protein orientation upright during the unfolding process, a time invariant "pivot-free" rotational potential as described in Kutzner et al. (2011) was applied throughout the whole simulation. We chose the Radial Motion 2 Alternative Potential. This particular choice of rotational potential has been developed to keep structural distortions of parts that moved away from or toward the rotation axis to a minimum (Kutzner et al., 2011). Simulations were carried out with a lower force constant of 5 kJ mol^{-1} nm^{-2} (0.0083 N/m) to allow small-scale tumbling as in a lipid bilayer, a correction factor $\varepsilon = 0.0001$ nm^2 to ensure a well-defined potential also close to the rotation axis, and a rotation rate of zero. The "pivot-free" variant of this potential used in this study eliminates the bias introduced by arbitrary choice of the pivot vector by defining the center of mass of the protein as pivot and computing the rotation potential accordingly.

Protein Rotation and Energy Landscape

Protein rigid-body rotation under mechanical load was described as deviation from initial orientation by Euler angles according to the roll-pitch-yaw convention (Figure 1F). Because the already unfolded amino acids were almost always perfectly aligned with the pulling direction, only protein structures remaining folded as described by the *Dictionary of the Secondary Structure of Proteins* (DSSP) (Joosten et al., 2011; Kabsch and Sander, 1983) were analyzed. For each snapshot, DSSP was applied, the output was analyzed with *do_dssp* (Hess et al., 2008), the rotation matrix with respect to the starting structure was determined with *g_rotmat* (Hess et al., 2008), and the Euler angles were computed from this rotation matrix.

To obtain an approximate energy landscape from our FPMD simulations, we integrated the force-distance curves of lipid membrane-embedded OmpG and solubilized OmpG and found two different unfolding energy potentials V_{embed} and V_{free}. Each point $\{d_i, \theta_i\}$ of the energy landscape (Figure 5) shows the approximate energy potential $V(d,\theta)$ as the average between these two effective energy potentials, weighted at any distance d by the deviation of $\theta_i(d)$ from the observed $\theta(d)$ from Figure S7. This approach suffers from a number of drawbacks, which we are well aware of: First, because our FPMD simulations are far from equilibrium, there is a lot of dissipative work exerted on the system, which we did not account for here. Second, for any given end-to-end distance d, a large number of different conformations are accessible, and we did not marginalize over all conformational coordinates compatible with that given d. For illustrative purposes, our approximation seems sufficient, however, and we obtained an unfolding energy landscape with energy barriers at plausible positions and shapes that together offer a unified view of all simulation results.

SUPPLEMENTAL INFORMATION

Supplemental Information includes eight figures and four movies and can be found with this article online at http://dx.doi.org/10.1016/j.str.2013.06.001.

ACKNOWLEDGMENTS

We thank C. Bippes, H. Gaub, F. Gräter, J. Helenius, and R. Newton for critical discussions. This project was supported by the Klaus-Tschira Foundation, the European Life Scientist Organization, the European Science Foundation EuroSYNBIO programme, and the Deutsche Forschungsgemeinschaft.

Received: March 25, 2013
Revised: June 1, 2013
Accepted: June 5, 2013
Published: July 3, 2013

REFERENCES

Berendsen, H.J.C., Postma, J.P.M., Van Gunsteren, W.F., DiNola, A., and Haak, J.R. (1984). Molecular dynamics with coupling to an external bath. J. Chem. Phys. *81*, 3684–3690.

Berendsen, H.J.C., Van Der Spoel, D., and Drunen, R.V. (1995). Gromacs: A message-passing parallel molecular dynamics implementation. Comput. Phys. Commun. *91*, 43–56.

Berger, O., Edholm, O., and Jähnig, F. (1997). Molecular dynamics simulations of a fluid bilayer of dipalmitoylphosphatidylcholine at full hydration, constant pressure, and constant temperature. Biophys. J. *72*, 2002–2013.

Berman, H.M., Westbrook, J., Feng, Z., Gilliland, G., Bhat, T.N., Weissig, H., Shindyalov, I.N., and Bourne, P.E. (2000). The protein data bank. Nucleic Acids Res. *28*, 235–242.

Bernstein, F.C., Koetzle, T.F., Williams, G.J., Meyer, E.F., Jr., Brice, M.D., Rodgers, J.R., Kennard, O., Shimanouchi, T., and Tasumi, M. (1977). The Protein Data Bank: a computer-based archival file for macromolecular structures. J. Mol. Biol. *112*, 535–542.

Bertz, M., Kunfermann, A., and Rief, M. (2008). Navigating the folding energy landscape of green fluorescent protein. Angew. Chem. Int. Ed. Engl. *47*, 8192–8195.

Bippes, C.A., and Muller, D.J. (2011). High-resolution atomic force microscopy and spectroscopy of native membrane proteins. Rep. Prog. Phys. *74*, 086601.

Bondar, A.-N., and White, S.H. (2012). Hydrogen bond dynamics in membrane protein function. Biochim. Biophys. Acta *1818*, 942–950.

Bonhivers, M., Desmadril, M., Moeck, G.S., Boulanger, P., Colomer-Pallas, A., and Letellier, L. (2001). Stability studies of FhuA, a two-domain outer membrane protein from Escherichia coli. Biochemistry *40*, 2606–2613.

Borgia, A., Williams, P.M., and Clarke, J. (2008). Single-molecule studies of protein folding. Annu. Rev. Biochem. *77*, 101–125.

Bosshart, P.D., Iordanov, I., Garzon-Coral, C., Demange, P., Engel, A., Milon, A., and Müller, D.J. (2012). The transmembrane protein KpOmpA anchoring the outer membrane of Klebsiella pneumoniae unfolds and refolds in response to tensile load. Structure *20*, 121–127.

Bowie, J.U. (2011). Membrane protein folding: how important are hydrogen bonds? Curr. Opin. Struct. Biol. *21*, 42–49.

Bussi, G., Donadio, D., and Parrinello, M. (2007). Canonical sampling through velocity rescaling. J. Chem. Phys. *126*, 014101.

Coskun, Ü., and Simons, K. (2011). Cell membranes: the lipid perspective. Structure *19*, 1543–1548.

Damaghi, M., Sapra, K.T., Köster, S., Yildiz, O., Kühlbrandt, W., and Muller, D.J. (2010b). Dual energy landscape: the functional state of the β-barrel outer membrane protein G molds its unfolding energy landscape. Proteomics *10*, 4151–4162.

Damaghi, M., Bippes, C., Köster, S., Yildiz, O., Mari, S.A., Kühlbrandt, W., and Muller, D.J. (2010a). pH-dependent interactions guide the folding and gate the transmembrane pore of the β-barrel membrane protein OmpG. J. Mol. Biol. *397*, 878–882.

Damaghi, M., Köster, S., Bippes, C.A., Yildiz, O., and Müller, D.J. (2011). One β hairpin follows the other: exploring refolding pathways and kinetics of the transmembrane β-barrel protein OmpG. Angew. Chem. Int. Ed. Engl. *50*, 7422–7424.

Darden, T., York, D., and Pedersen, L. (1993). Particle mesh Ewald—An N.Log(N) method for ewald sums in large systems. J. Chem. Phys. *98*, 10089–10092.

Dietz, H., and Rief, M. (2004). Exploring the energy landscape of GFP by single-molecule mechanical experiments. Proc. Natl. Acad. Sci. USA *101*, 16192–16197.

Dietz, H., and Rief, M. (2006). Protein structure by mechanical triangulation. Proc. Natl. Acad. Sci. USA *103*, 1244–1247.

Dudko, O.K., Filippov, A.E., Klafter, J., and Urbakh, M. (2003). Beyond the conventional description of dynamic force spectroscopy of adhesion bonds. Proc. Natl. Acad. Sci. USA *100*, 11378–11381.

Dudko, O.K., Hummer, G., and Szabo, A. (2006). Intrinsic rates and activation free energies from single-molecule pulling experiments. Phys. Rev. Lett. *96*, 108101.

Engel, A., and Gaub, H.E. (2008). Structure and mechanics of membrane proteins. Annu. Rev. Biochem. *77*, 127–148.

Engelman, D.M. (2005). Membranes are more mosaic than fluid. Nature *438*, 578–580.

Engelman, D.M., Chen, Y., Chin, C.-N., Curran, A.R., Dixon, A.M., Dupuy, A.D., Lee, A.S., Lehnert, U., Matthews, E.E., Reshetnyak, Y.K., et al. (2003). Membrane protein folding: beyond the two stage model. FEBS Lett. *555*, 122–125.

Evans, E. (1998). Energy landscapes of biomolecular adhesion and receptor anchoring at interfaces explored with dynamic force spectroscopy. Faraday Discuss. *111*, 1–16.

Evans, E. (2001). Probing the relation between force—lifetime—and chemistry in single molecular bonds. Annu. Rev. Biophys. Biomol. Struct. *30*, 105–128.

Evans, E., and Ritchie, K. (1997). Dynamic strength of molecular adhesion bonds. Biophys. J. *72*, 1541–1555.

Gräter, F., Shen, J., Jiang, H., Gautel, M., and Grubmüller, H. (2005). Mechanically induced titin kinase activation studied by force-probe molecular dynamics simulations. Biophys. J. *88*, 790–804.

Grubmüller, H., Heymann, B., and Tavan, P. (1996). Ligand binding: molecular mechanics calculation of the streptavidin-biotin rupture force. Science *271*, 997–999.

Haswell, E.S., Phillips, R., and Rees, D.C. (2011). Mechanosensitive channels: what can they do and how do they do it? Structure *19*, 1356–1369.

Hess, B., Bekker, H., Berendsen, H., and Fraaije, J. (1997). LINCS: A linear constraint solver for molecular simulations. J. Comput. Chem. *18*, 1463–1472.

Hess, B., Kutzner, C., van der Spoel, D., and Lindahl, E. (2008). GROMACS 4: Algorithms for highly efficient, load-balanced, and scalable molecular simulation. J. Chem. Theory Comput. *4*, 435–447.

Hooft, R.W.W., Sander, C., and Vriend, G. (1996). Positioning hydrogen atoms by optimizing hydrogen-bond networks in protein structures. Proteins *26*, 363–376.

Hoover, W.G. (1985). Canonical dynamics: Equilibrium phase-space distributions. Phys. Rev. A *31*, 1695–1697.

Isralewitz, B., Izrailev, S., and Schulten, K. (1997). Binding pathway of retinal to bacterio-opsin: a prediction by molecular dynamics simulations. Biophys. J. *73*, 2972–2979.

Joosten, R.P., te Beek, T.A.H., Krieger, E., Hekkelman, M.L., Hooft, R.W.W., Schneider, R., Sander, C., and Vriend, G. (2011). A series of PDB related databases for everyday needs. Nucleic Acids Res. *39*(Database issue), D411–D419.

Jorgensen, W., and Tiradorives, J. (1988). The OPLS potential functions for proteins - energy minimizations for crystals of cyclic peptides and crambin. J. Am. Chem. Soc. *110*, 1657–1666.

Kabsch, W., and Sander, C. (1983). Dictionary of protein secondary structure: pattern recognition of hydrogen-bonded and geometrical features. Biopolymers *22*, 2577–2637.

Kedrov, A., Janovjak, H., Sapra, K.T., and Müller, D.J. (2007). Deciphering molecular interactions of native membrane proteins by single-molecule force spectroscopy. Annu. Rev. Biophys. Biomol. Struct. *36*, 233–260.

Kutzner, C., Czub, J., and Grubmüller, H. (2011). Keep it flexible: Driving macromolecular rotary motions in atomistic simulations with GROMACS. J. Chem. Theory Comput. *7*, 1381–1393.

Lee, G., Abdi, K., Jiang, Y., Michaely, P., Bennett, V., and Marszalek, P.E. (2006). Nanospring behaviour of ankyrin repeats. Nature *440*, 246–249.

Lee, W., Zeng, X., Rotolo, K., Yang, M., Schofield, C.J., Bennett, V., Yang, W., and Marszalek, P.E. (2012). Mechanical anisotropy of ankyrin repeats. Biophys. J. *102*, 1118–1126.

Lindorff-Larsen, K., Piana, S., Palmo, K., Maragakis, P., Klepeis, J.L., Dror, R.O., and Shaw, D.E. (2010). Improved side-chain torsion potentials for the Amber ff99SB protein force field. Proteins *78*, 1950–1958.

Lingwood, D., and Simons, K. (2010). Lipid rafts as a membrane-organizing principle. Science *327*, 46–50.

Mari, S.A., Köster, S., Bippes, C.A., Yildiz, O., Kühlbrandt, W., and Muller, D.J. (2010). pH-induced conformational change of the beta-barrel-forming protein OmpG reconstituted into native E. coli lipids. J. Mol. Biol. *396*, 610–616.

Mickler, M., Dima, R.I., Dietz, H., Hyeon, C., Thirumalai, D., and Rief, M. (2007). Revealing the bifurcation in the unfolding pathways of GFP by using single-molecule experiments and simulations. Proc. Natl. Acad. Sci. USA *104*, 20268–20273.

Miyamoto, S., and Kollman, P. (1992). SETTLE—an analytical version of the SHAKE and RATTLE algorithm for rigid water models. J. Comput. Chem. *13*, 952–962.

Nosé, S. (1984). A molecular dynamics method for simulations in the canonical ensemble. Mol. Physiol. *52*, 255–268.

Nunes, J.M., Hensen, U., Ge, L., Lipinsky, M., Helenius, J., Grubmüller, H., and Muller, D.J. (2010). A "force buffer" protecting immunoglobulin titin. Angew. Chem. Int. Ed. Engl. *49*, 3528–3531.

Onuchic, J.N., and Wolynes, P.G. (2004). Theory of protein folding. Curr. Opin. Struct. Biol. *14*, 70–75.

Parrinello, M. (1981). Polymorphic transitions in single crystals: A new molecular dynamics method. J. Appl. Physiol. *52*, 7182–7190.

Puchner, E.M., Alexandrovich, A., Kho, A.L., Hensen, U., Schäfer, L.V., Brandmeier, B., Gräter, F., Grubmüller, H., Gaub, H.E., and Gautel, M. (2008). Mechanoenzymatics of titin kinase. Proc. Natl. Acad. Sci. USA *105*, 13385–13390.

Sapra, K.T., Damaghi, M., Köster, S., Yildiz, O., Kühlbrandt, W., and Muller, D.J. (2009). One beta hairpin after the other: exploring mechanical unfolding pathways of the transmembrane beta-barrel protein OmpG. Angew. Chem. Int. Ed. Engl. *48*, 8306–8308.

Sheetz, M.P. (2001). Cell control by membrane-cytoskeleton adhesion. Nat. Rev. Mol. Cell Biol. *2*, 392–396.

Sukharev, S., and Sachs, F. (2012). Molecular force transduction by ion channels: diversity and unifying principles. J. Cell Sci. *125*, 3075–3083.

Thoma, J., Bosshart, P., Pfreundschuh, M., and Müller, D.J. (2012). Out but not in: the large transmembrane β-barrel protein FhuA unfolds but cannot refold via β-hairpins. Structure *20*, 2185–2190.

Tieleman, D.P. (2011). Lipid structures and topologies data bank. http://moose.bio.ucalgary.ca/index.php?page=Structures_and_Topologies. Retrieved June 2011.

Vriend, G. (1990). WHAT IF: a molecular modeling and drug design program. J. Mol. Graph. *8*, 52–56, 29.

White, S.H., and Wimley, W.C. (1999). Membrane protein folding and stability: physical principles. Annu. Rev. Biophys. Biomol. Struct. *28*, 319–365.

Wolfram Research, Inc.. (2010). Mathematica Edition: Version 8.0 (Champaign, IL: Wolfram Research, Inc.).

Wolf, M.G., Hoefling, M., Aponte-Santamaría, C., Grubmüller, H., and Groenhof, G. (2010). g_membed: Efficient insertion of a membrane protein into an equilibrated lipid bilayer with minimal perturbation. J. Comput. Chem. *31*, 2169–2174.

Yang, F., Moss, L.G., and Phillips, G.N., Jr. (1996). The molecular structure of green fluorescent protein. Nat. Biotechnol. *14*, 1246–1251.

Yildiz, O., Vinothkumar, K.R., Goswami, P., and Kühlbrandt, W. (2006). Structure of the monomeric outer-membrane porin OmpG in the open and closed conformation. EMBO J. *25*, 3702–3713.

